

H4K20me0 recognition by BRCA1-BARD1 directs homologous recombination in sister chromatids

Kyosuke Nakamura^{1,2,12}, Giulia Saredi^{1,3,12}, Jordan R. Becker^{4,12}, Benjamin M. Foster^{5,6,7}, Nhuong V. Nguyen^{6,7,8}, Tracey Beyer^{1,2}, Laura C. Cesa^{1,2}, Peter A. Faull^{6,9}, Saulius Lukauskas^{5,6,10}, Thomas Frimurer¹¹, J. Ross Chapman⁴, Till Bartke^{5,6,7,*} and Anja Groth^{1,2,*}

¹Biotech Research and Innovation Centre (BRIC), University of Copenhagen, Faculty of Health Sciences, University of Copenhagen, 2200 Copenhagen, Denmark. ²The Novo Nordisk Foundation Center for Protein Research (CPR), University of Copenhagen, Faculty of Health Sciences, University of Copenhagen, 2200 Copenhagen, Denmark. ³Current address: MRC Protein Phosphorylation and Ubiquitylation Unit, School of Life Sciences, Sir James Black Centre, University of Dundee, Dundee DD1 5EH, Scotland. ⁴Wellcome Centre For Human Genetics, Roosevelt Drive, Oxford, OX3 7BN, UK. ⁵Institute of Functional Epigenetics, Helmholtz Zentrum München, 85764 Neuherberg, Germany. ⁶MRC London Institute of Medical Sciences (LMS), Du Cane Road, London W12 0NN, UK. ⁷Institute of Clinical Sciences (ICS), Faculty of Medicine, Imperial College London, Du Cane Road, London W12 0NN, UK. ⁸Current address: Friedrich Miescher Institute for Biomedical Research (FMI), Maulbeerstr. 66, 4058 Basel, Switzerland. ⁹Current address: The Francis Crick Institute, 1 Midland Road, London NW1 1AT, UK. ¹⁰Department of Chemical Engineering, Imperial College London, London SW7 2AZ, UK. ¹¹The Novo Nordisk Foundation Center for Basic Metabolic Research, University of Copenhagen, Faculty of Health Sciences, University of Copenhagen, 2200 Copenhagen, Denmark.

¹²These authors contributed equally to this work.

*Correspondence should be addressed to T.B. (till.bartke@helmholtz-muenchen.de) and A.G. (anja.groth@bric.ku.dk).

Genotoxic DNA double-strand breaks (DSBs) can be repaired by error-free homologous recombination (HR) or mutagenic non-homologous end-joining (NHEJ)¹. HR suppresses tumorigenesis¹, but is restricted to S and G2 phase of the cell cycle when a sister chromatid is present². BRCA1 promotes HR by antagonizing the anti-resection factor 53BP1²⁻⁵, but it remains

unknown how BRCA1 function is limited to S and G2 phase. We show that BRCA1 recruitment requires recognition of histone H4 unmethylated at lysine 20 (H4K20me0), linking DSB repair pathway choice directly to sister chromatid availability. We identify the ankyrin repeat domain (ARD) of BARD1, the obligate BRCA1 binding partner³, as a reader of H4K20me0 present on new histones in post-replicative chromatin⁶. BARD1 ARD mutations disabling H4K20me0 recognition abrogate accumulation of BRCA1 at DSBs, causing aberrant build-up of 53BP1 and allowing anti-resection activity to prevail in S and G2. Consequently, BARD1 recognition of H4K20me0 is required for HR and resistance to PARP inhibitors. Collectively, this reveals that BRCA1-BARD1 monitors the replicative state of the genome to oppose 53BP1 function, routing only DSBs within sister chromatids to HR.

Histone H4K20 methylation oscillates during the cell cycle with major implications for chromosome replication, condensation and stability⁷. In G1 phase, nucleosomes are fully methylated at H4K20, with >80% carrying H4K20me2⁶. During S phase, new histones unmethylated at H4K20 are incorporated on newly synthesized DNA and mixed in a 1:1 ratio with old nucleosomes methylated at H4K20. H4K20me0 thereby marks the post-replicative state of a genomic locus and thus the presence of a sister chromatid until G2/M⁶, when a surge of SET8 methyltransferase activity catalyses H4K20me1 that is subsequently converted to me2/3 by SUV4-20^{6, 7}. The cell exploits this to regulate the recruitment of DNA repair factors. The TONSL-MMS22L HR⁸ complex reads H4K20me0 via its ARD to direct its function in RAD51 loading⁹ to collapsed replication forks and DSBs in post-replicative chromatin⁶. Conversely, the NHEJ-promoting factor 53BP1 recognizes H4K20me1/2¹⁰ present on old histones throughout the cell cycle⁶. 53BP1 accumulation at DSBs is reduced in post-replicative chromatin¹¹⁻¹³, correlating with the replication-dependent dilution of H4K20me1/2^{6, 12, 13}. However, H4K20me1/2 dilution cannot explain 53BP1 suppression and the shift to HR, as BRCA1 is required to antagonize 53BP1 accumulation at DSBs in S/G2^{11, 12}. DNA damage induced ubiquitylation by RNF8 and RNF168 is required for both 53BP1 and BRCA1 recruitment¹⁴ and these signalling pathways are not cell cycle specific¹⁴. The crucial question of how BRCA1 specifically recognizes post-replicative chromatin thus remains a missing part in the puzzle to understand DSB repair pathway choice.

Because H4K20me0 directly marks sister chromatid availability, we set out to comprehensively

explore its function. Using an unbiased quantitative proteomic strategy to identify proteins specifically recognizing nucleosomes carrying H4K20me0, we identified almost exclusively three post-replication DNA repair complexes; a BRCA1-BARD1 containing complex involved in HR³, the RAD18-SLF1-SLF2 complex implicated in interstrand cross-link repair¹⁵, and TONSL-MMS22L as expected⁶ (Fig. 1a). Consistent with previous work^{7, 16}, ORCA/LRWD1, ORC1, ORC2 and ORC3 were specifically enriched on nucleosomes carrying H4K20me2 (Fig 1a). Intriguingly, BARD1 and SLF1 both contain ARDs with high similarity to the TONSL ARD that recognizes H4K20me0⁶ (Fig. 1b, Supplementary Fig. 1), and the reported structure of the BARD1 ARD¹⁷ revealed that the histone H4 binding interface⁶ is structurally conserved (Fig. 1b). BARD1 and SLF1 showed a clear preference for H4K20me0 over H4K20me2 marked nucleosomes in pull-down experiments (Fig. 1c) and, importantly, mutation of three residues predicted to bind H4K20me0 (ARD 3A) based on TONSL homology abrogated nucleosome binding by SLF1 and BARD1 (Fig. 1b, d). These data identify two new H4K20me0 readers and argue for a general role of H4K20me0 in promoting post-replication DNA repair. In particular, recognition of H4K20me0 by BARD1 could provide a mechanism for BRCA1 recruitment to post-replicative chromatin and directly link induction of HR to sister chromatid availability. Here, we explore this hypothesis.

As H4K20me0 marks post-replicative chromatin irrespective of DNA lesions⁶, BRCA1-BARD1 might bind post-replicative chromatin in unperturbed cells. Indeed, we found progressive accumulation of the BRCA1-BARD1 complex on chromatin during S phase mirroring H4K20me0 incorporation⁶ (Fig. 2a; Supplementary Fig. 2a, b), and this was dependent on H4K20me0 recognition by the BARD1 ARD (Fig. 2b; Supplementary Fig. 2c, d, e). BARD1 localized to EdU pulse-labelled replication foci in early S phase, but co-localization decreased in mid and late S phase (Fig. 2c). With continuous EdU labelling of post-replicative DNA, BARD1 and EdU co-localization remained high throughout S phase (Fig. 2c) consistent with recruitment of BARD1 via H4K20me0 present both at sites of ongoing replication and in post-replicative chromatin⁶. Depletion of SET8, responsible for methylation of H4K20 in G2 and mitosis, increased H4K20me0 levels and augmented BRCA1-BARD1 binding to chromatin in G2 and G1 in a manner dependent on H4K20me0 recognition by the BARD1 ARD (Fig. 2d; Supplementary Fig. 2f, g, h). SET8 depleted cells show reduced NHEJ and elevated rates of HR and ssDNA annealing¹⁸, but due to pleiotropic defects such as chromatin decompaction and DNA damage, this system was unsuitable for testing the role of

H4K20me0 recognition in supporting BRCA1-BARD1-dependent HR. Taken together, our results establish ARD-dependent recognition of H4K20me0 as a mechanism for general pre-lesion recruitment of BRCA1-BARD1 to post-replicative chromatin irrespective of DNA damage.

Next, we analysed the role of H4K20me0 binding by BARD1 ARD in DNA DSB repair. Wild-type (WT) BARD1 recruitment to ionizing irradiation (IR)-induced DSBs increased during S phase and reached a maximum in late S before dropping in G2/M (Fig. 3a), mirroring H4K20me0 occupancy⁶ (Supplementary Fig. 2a) and recruitment of other HR factors^{11, 19}. Importantly, mutation of the BARD1 ARD ablated recruitment of both BARD1 and BRCA1 to DSBs in S phase (Fig. 3a, b). Of note, BARD1 WT and ARD mutants were expressed at similar levels across the cell cycle and were proficient for BRCA1 stabilization via the RING domain dimerization³ (Supplementary Fig. 2c, e). Further, we found that ARD recognition of H4K20me0 was as important as RNF8-dependent ubiquitination¹⁴ for BRCA1 accumulation at DSBs (Supplementary Fig. 3a), indicating that BRCA1-BARD1 recruitment requires multivalent interactions with chromatin at DSBs, similar to 53BP1²⁰. Our finding that H4K20me0 is essential for BRCA1-BARD1 recruitment explains why forced methylation of H4K20 by non-degradable SET8 blocks BRCA1 recruitment and RAD51 loading at DSBs in S phase¹². Collectively, this establishes H4K20me0 recognition as the critical mechanism underlying specific recruitment of BRCA1 to DSBs in S phase and assigns a primary function to the BARD1 ARD.

A key essential activity of BRCA1 is to oppose the anti-resection activity of 53BP1^{4, 5, 11, 12} to direct DSBs towards HR. 53BP1 accumulation at DSBs is dependent on recognition of H4K20me1/2 by its Tudor domain and RNF168-dependent mono-ubiquitination of H2AK15¹⁴. However, BRCA1 can prevent 53BP1 access to repair sites^{11, 12}. We therefore hypothesized that BARD1 recognition of H4K20me0 might target BRCA1-BARD1-dependent exclusion of 53BP1 to post-replicative chromatin. BRCA1 foci dominated in mid and late S phase in the presence of BARD1 WT as expected¹¹, but, remarkably, this pattern was reversed by the BARD1 ARD mutant (Supplementary Fig. 3b). The BARD1 ARD mutant also completely failed to suppress 53BP1 accumulation at DSBs in BARD1 depleted S phase cells (Fig. 3c, d). This switch from BRCA1-BARD1 to 53BP1 dominance ablated DNA end-resection (Fig. 3e) and RAD51 loading (Fig. 3f), indicating that BARD1 ARD mutant cells cannot route DSBs to HR. These results demonstrate that BARD1 ARD

recognition of H4K20me0 is required to recruit BRCA1 and curb 53BP1 anti-resection activity at DSBs in S phase.

To address the implications for HR directly, we took advantage of the DR-GFP HR reporter²¹ using both U-2-OS cells depleted for endogenous BARD1 and a *BARD1*-null mouse mammary carcinoma cell line²². Mutation of the ARD ablated BARD1 function in HR in both systems (Fig. 4a, b). Consistent with a role of the H4K20me0 recognition in antagonizing 53BP1, depletion of 53BP1 partly restored HR in cells expressing the ARD mutant (Supplementary Fig. 3c). Moreover, mutation of the H4K20me0 recognition site was as detrimental to HR as deletion of the full ARD or BRCT domain previously shown to be essential for HR²² (Fig. 4b, Supplementary Fig. 3d), underscoring that the essential function of the ARD in HR is H4K20me0 recognition. In these experiments we included mouse BARD1 as a control and found that it rescued HR activity (Supplementary Fig. 3d) although N470, predicted to bind H4K20me0 (Fig. 1b), is not conserved in mice. This suggested that the H4K20me0 reader domains in BARD1 and TONSL differ with respect to some H4 tail interactions. Taking advantage of the high resolution structures of the TONSL ARD-H3-H4⁶ complex and the BARD ARD¹⁷, we used the Rosetta modelling package to exhaustively model the structure of the BARD1 ARD-H3-H4 complex. The best scoring structures predicted a repositioning of H4 R17, reducing the contacts between the H4 tail and BARD1 N470 as compared to N571 in TONSL (Supplementary Fig. 4a, b). All other interactions were highly similar between the two reader domains, in particular the contacts between BARD1 E467 and D500 with H4 H18 and the contacts between BARD1 E429, D458 and E467 with H4 K20 were conserved (Supplementary Fig. 4a, b). Consistent with this binding model, residues E467 and D500, but not N470, were critical for BARD1 chromatin binding and recruitment to IR-induced DSBs (Supplementary Fig. 4c, d). These key acidic residues diverge from the consensus ankyrin repeat¹⁷, but are conserved across species in BARD1, TONSL and SLF1 (Supplementary Fig. 4e), explaining specialization of these ARDs for H4K20me0 recognition.

Many mutations in the BARD1 ARD have been identified in cancer and our structural model pinpoint those with potential to disrupt H4K20me0 binding and promote carcinogenesis by crippling HR (Fig. 4c). HR deficiency is exploited in the treatment of tumours with BRCA1 and BRCA2 mutations²³ as it sensitizes tumour cells to PARP inhibitors (PARPi). Defects in H4K20me0

recognition are therefore expected to sensitize cells to PARPi treatment. Consistent with this prediction, a functional H4K20me0 recognition interface was required for BARD1 to rescue sensitivity to PARPi in BARD1-depleted cells (Fig. 4d) and the BARD1 ARD mutant even impaired HR and sensitized cells to PARPi in a dominant negative manner (Fig. 4e, f), underscoring that H4K20me0 recognition is essential to BRCA1-BARD1 function in HR.

A role for the BARD1-BRCA1 E3 ubiquitin ligase activity in promoting HR was also recently reported and proposed to stimulate nucleosome remodeling events that inhibit 53BP1-dependent chromatin binding at DSB sites²⁴. We therefore sought to determine the relative importance of H4K20me0 recognition in supporting BRCA1-BARD1-dependent HR, over BARD1 dependent enzymatic E3 ubiquitin ligase activity. We generated a human conditional BARD1 knockout cell line by tagging both alleles of BARD1 with a C-terminal Auxin-Induced-Degron (AID)²⁵, *BARD1^{AID/AID}* (Fig. 5a), and stably expressed a BARD1 WT and mutant transgenes. In *BARD1^{AID/AID}* HCT116 cells, doxycycline-induced expression of *OsTIR1* transgenes, integrated in the *AAVSI* locus, allowed for efficient and stable depletion of endogenous BARD1 upon the addition of the auxin indole-3-acetic acid (IAA; Fig. 5a). IAA-induced degradation of BARD1 resulted in BRCA1 de-stabilization (Fig. 5a) and PARPi hypersensitivity (Fig. 5b). The de-stabilization of BRCA1, was equally bypassed in cells expressing wild type and mutant BARD1 transgenes (Fig. 5c). In addition to the recently reported BARD1 R99E RING-domain mutant and BARD1 ARD 3A, we included a BARD1 BRCT-domain mutant (K619A)²⁶ that abrogates poly(ADP-ribose)-dependent recruitment of BARD1 to stalled replication forks but is proficient for HR in mice²⁷. In control (GST-expressing) *BARD1^{AID/AID}* cells, IAA-treatment resulted in an acute hypersensitivity to PARPi (Fig. 5d). This hypersensitivity was completely reversed by the expression of wild type BARD1, or the BARD1^{R99E} and BARD1^{K619A} mutants (Fig. 5d). In contrast, BARD1 ARD 3A expression failed to suppress PARPi-sensitivity (Fig. 5d). These data indicate that ARD-mediated H4K20me0 binding represents a prime function for BARD1 in HR, while the E3-ligase activity and PAR-binding are dispensable, consistent with these activities not being required for tumor suppression in mice^{27, 28}.

How cells switch from mutagenic NHEJ to error-free HR during S and G2 has been a long-standing question. Our results provide a simple solution in which ARD recognition of H4K20me0 triggers BRCA1-BARD1 recruitment specifically to post-replicative chromatin to antagonize 53BP1 and promote resection only when a sister chromatid is available for HR (Fig. 5e). This pre-lesion *cis*-

acting mechanism acts at the most upstream point in repair pathway choice prior to cell cycle regulation of end-resection²⁹ and BRCA2 recruitment³⁰ as well as H4K20me0-mediated RAD51 loading via TONSL-MMS22L⁶. We propose that two complementary mechanisms control HR in mammalian cells, sister chromatid sensing via H4K20me0 (this work and⁶) and cell cycle regulation² that is well-established. Consistent with this, HR is strongly impaired when deposition of new histones and thus marking of post-replicative chromatin by H4K20me0 is attenuated³¹. Recognition of H4K20me0 on new histones by BARD1, contrary to recognition of H4K20me1/2 on old histones by 53BP1, explains the specific recruitment of BRCA1 to DSBs in S/G2, including the competition between pro- and anti-resection activities at lesions in S/G2 chromatin³² where H4K20me0 and H4K20me1/2 marked nucleosomes co-exist. At break sites H4K20 binding is integrated with additional signals, as both 53BP1²⁰ and BRCA1-BARD1³³⁻³⁵ (this work) rely on multivalent binding for accumulation at DSBs including RNF8- and RNF168-dependent ubiquitination¹⁴. This cross-talk between the pathways with respect to ubiquitin signaling remains enigmatic but suggests a constant competition for chromatin binding between 53BP1 and BRCA1-BARD1 that converges at DSBs and is tuned to the replicative state of a genomic locus by H4K20 methylation status. Competition for ubiquitin binding at DSBs may also explain the futile recruitment of BRCA1 to DSBs in G1 cells that lack 53BP1³⁶. In the presence of 53BP1, recognition of H4K20me0 provides BRCA1-BARD1 with an advantage in post-replicative chromatin, tipping the balance towards 53BP1 exclusion and induction of HR, which is then executed by downstream cell-cycle regulated factors. Our data argue that ARD recognition of H4K20me0 mediates an essential HR function of BARD1, providing first molecular insight into the function of the highly conserved ARD and identifying the enigmatic HR function of BARD1 beyond BRCA1 stabilization³⁷. Our work explains how the availability of a sister chromatid substrate for HR directs repair pathway choice, and the druggability of histone reader domains³⁸ suggests that this mechanism can be exploited for targeting BRCA1 in cancers addicted to HR.

Supplementary Information is available online.

Acknowledgements

We thank Jiri Lukas for commenting on the manuscript, the Groth lab for fruitful discussions, Richard Baer for sharing the BARD1 plasmid and *BARD1*-null mouse mammary carcinoma cells,

Masato Kanemaki for OsTIR1 antibody, Yasuko Antoku for assistance with microscopy and Jens V. Johansen for help with statistical analysis. J.R.B. is funded by a Cancer Research UK Career Development Grant awarded to J.R.C. (C52690/A19270). Funding for T.B. was provided by the Medical Research Council (Grant no. MC_UP_1102/2) and the European Research Council (ERC StG no. 309952), S.L. was supported by a stipend from the Biotechnology and Biological Sciences Research Council. The Groth lab is supported by the Danish Cancer Society, the Novo Nordisk Foundation, the Lundbeck Foundation, the European Research Council (ERC CoG no. 724436), the Independent Research Fund Denmark, and the NEYE Foundation.

Author Contributions

K.N., G.S. and A.G. conceived the study and K.N. carried out the functional analysis. G.S. performed pull-downs with endogenous BARD1 and SLF1, and established tools and reagents. J.R.B. generated and carried out experiments with BARD1^{AID/AID} cells. B.M.F. prepared materials for nucleosome pull-downs. N.N. prepared materials, carried out SILAC nucleosome pull-down experiments and analysed data. T.E.B. and L.C.C. performed pull-downs with BARD1 and SLF1 mutants. P.A.F. carried out mass spectrometry measurements and analysed mass spectrometry data. S.L. performed bioinformatics analyses of mass spectrometry data. T.F. performed structural modelling. J.R.C., T.B. and A.G. supervised the project and analysed data. G.S. and A.G. wrote the manuscript with input from all authors.

Materials and Correspondence. Correspondence and materials requests should be addressed to T.B. (till.bartke@helmholtz-muenchen.de) and A.G. (anja.groth@bric.ku.dk).

Competing financial interests

G.S. and A.G. are inventors on a filed patent application covering the therapeutic targeting of ARD interactions with H4K20me0 for cancer therapy. A.G. and T.F. are co-founders of Ankrin Therapeutics.

Figure Legends

Figure 1. BARD1 and SLF1 recognize nucleosomes carrying H4K20me0 via their ARDs. a, Pull-downs from HeLa nuclear extracts with differentially modified biotinylated recombinant di-

nucleosomes analysed by SILAC-based mass spectrometry. **b**, Alignment of the TONSL ARD (aa. 528-626), BARD1 ARD (aa. 427-546) and SLF1 ARD (aa. 806-903) (left). Overlay of the BARD1 ARD¹⁷ structure with the TONSL ARD from the TONSL-ARD-MCM2-HBD-H3-H4 structure⁶ (right). Asterisks indicate the amino acids mutated in ARD 3A in **d**. **c**, Pull-downs with modified biotinylated di-nucleosomes in HeLa nuclear extracts. Representative of 3 biological replicates. **d**, Pull-downs with biotinylated di-nucleosomes in nuclear extracts from HeLa cells expressing either WT or ARD 3A mutant forms of BARD1 or SLF1. Representative of 3 (BARD1) and 2 (SLF1) biological replicates. Unprocessed blots for **c** and **d** are presented in Supplementary Fig. 5.

Figure 2. ARD recognition of H4K20me0 recruits BRCA1-BARD1 to post-replicative chromatin. **a**, High content microscopy of chromatin-bound BARD1 and BRCA1 in pre-extracted U-2-OS cells pulsed with EdU. Cell cycle stages were defined by gating on EdU and DAPI (upper right). Mean intensities are shown relative to G1 levels with S.D., $n=3$ independent experiments; from left $P=0.0203, 0.0057, 0.0076, 0.017, 0.0055, 0.0315, 0.0251, 0.0821, \text{NS}$, not significant, ratio paired two-sided t -test. Data points represent the mean of >173 cells. The correlation between BARD1 and BRCA1 mean intensities (lower right) is shown with Pearson R^2 correlation ($P < 0.0001$). Representative cells are shown; scale bar, $10\ \mu\text{m}$. **b**, High content microscopy of chromatin-bound Flag-HA-BARD1 in U-2-OS inducible for Flag-HA-BARD1 WT or ARD 3A. Mean is shown with S.D., $n=3$ independent experiments; from left $P=0.0214, 0.0036, 0.022, 0.0204, 0.0074$), ratio paired two-sided t -test. Data points represent the mean of >254 cells. **c**, Co-localization of chromatin-bound BARD1 and EdU in cells pulsed with EdU (left) or released into S phase in the presence of EdU (right). S-phase stages were defined by EdU, DAPI and MCM2 staining⁶. Drawings illustrate the expected results based on H4K20me0 distribution⁶. Error bars indicate S.D. with mean. From left, $n=28, 22, 18$, and $18, 25, 22$ cells; representative cells are shown. Data were derived from two independent experiments. ****, $P < 0.0001$, by the Mann-Whitney test (two-sided). NS, not significant (from left $P=0.1392$ and 0.4494). Scale bar, $15\ \mu\text{m}$. **d**, BARD1 and BRCA1 chromatin-binding in G1 and G2 phase in SET8-depleted cells. Cells inducible for siRNA resistant Flag-HA-BARD1 WT or ARD 3A were treated with BARD1 and SET8 siRNAs and analysed as in **a**. Mean intensity in SET8 and BARD1 co-depletion cells over BARD1 depletion alone with S.D. is shown, $n=3$ independent experiments; from left $P=0.0048, 0.0021, 0.013, 0.0009$), ratio paired two-sided t -test. Data points represent the mean of >206 cells.

Figure 3. H4K20me0 recognition is required for BRCA1-BARD1 recruitment to DSBs, 53BP1 antagonization, and end-resection. a, High content microscopy of Flag-HA-BARD1 accumulation at IR-induced DNA DSBs. U-2-OS cells expressing Flag-HA-BARD1 WT or ARD 3A were pulsed with EdU, irradiated with 1 Gy and 45 minutes later pre-extracted and analysed by immunofluorescence. Foci number is shown relative to BARD1 WT in mid S. S phase stages were defined as in Fig. 2a. The mean is shown with S.D., $n=3$ independent experiments. Data points represent the mean of >381 cells. Scale bar, 10 μ m. **b, c,** BRCA1 (**b**) and 53BP1 (**c**) accumulation at IR-induced DSBs in U-2-OS cells treated with control (Ctrl) or BARD1 siRNAs and induced with tetracycline (TET) to express siRNA-resistant Flag-HA-BARD1 WT or ARD 3A. Cells were analysed as in **a** and late S phase cells are shown. Mean shown as '+', whiskers indicate 10-90 percentile; from left (**b**), $n = 1068, 723, 1224, 896, 1420, 627, 902, 597$ cells; from left (**c**), $n = 1068, 723, 1224, 896, 1420, 627, 902, 597$ cells. **d,** BRCA1 and 53BP1 foci in single cells in late S phase analysed as in **b** and **c**. BARD1 WT $n=896$; BARD1 ARD 3A $n=597$. **e,** High content microscopy of ssDNA measured by BrdU staining under non-denaturing conditions in U-2-OS cells treated with siRNA and TET as in **c**. Cells with high (top 15%) and low (bottom 15%) H4K20me0 levels (defined by gating on mean intensity) are shown. Cells were fixed 3 hours after IR (3 Gy). Mean shown as '+', whiskers indicate 10-90 percentile; from left, $n = 503, 442, 371, 312, 474, 269, 381, 330$ and $617, 641, 316, 237, 540, 495, 277, 194$ cells. **f,** High-content microscopy of IR-induced RAD51 foci analysed as in **b**. Mean shown as '+', whiskers indicate 10-90 percentile; from left, $n = 310, 384, 327, 326, 329, 295, 321, 331$ cells.

Figure 4. BARD1 recognition of H4K20me0 is required for HR and PARPi resistance. a, HR efficiency measured in DR-GFP U-2-OS cells treated with control (Ctrl) or BARD1 siRNA and complemented with siRNA-resistant BARD1 WT, ARD 3A or empty vector. The HR efficiency is shown as % of control siRNA. Mean with S.D., $n=3$ independent experiments, from left, $P=0.29, 0.0016$; NS, not significant by ratio paired two-sided t -test. **b,** HR efficiency measured in *BARD1*-null mouse mammary carcinoma cells carrying a DR-GFP reporter and complemented as indicated. The HR efficiency relative to empty vector is indicated above each bar. Mean with S.D., $n=3$ independent experiments. **c,** BARD1 ARD mutations identified by cancer genome sequencing (COSMIC <https://cancer.sanger.ac.uk/cosmic>; TCGA Research Network:

<https://cancergenome.nih.gov/>. Mutations H459Y, D458V and E467K are predicted to disturb H4 binding, as the residues are directly involved in H4 binding (red). Mutations D495Y, K503T, T534V and K540T are prone to affect the structural integrity of BARD1 ARD since the wild type residues are involved in intra-molecular hydrogen bonding (orange). Mutations buried in the core (A435V, L447F, L480S, L498I and P530S; dark green) might affect the structure of the ARD and thus indirectly disrupt H4 binding. Surface exposed mutations (light green) are less likely to affect ARD structure and H4 binding. **d**, Sensitivity to Olaparib analysed by colony formation in siRNA-treated U-2-OS cells induced for expression of siRNA-resistant Flag-HA-BARD1 WT or ARD 3A. Mean with S.D., $n=3$ independent experiments. **e, f**, BARD ARD mutations impair HR and sensitize cells to PARPi in a dominant negative manner. (**e**) HR efficiency measured in U-2-OS cells carrying a DR-GFP reporter, transfected with the indicated BARD1 constructs or empty vector along with an I-SceI expression vector. Mean with S.D., $n=4$ independent experiments. *, $P=0.0136$, ratio paired two-sided t -test. (**f**) Colony formation upon Olaparib (1 μ M) treatment of U-2-OS cells induced to express Flag-HA-BARD1 WT and ARD 3A expression by tetracycline (TET). $n=3$ independent experiments, mean is shown. **, $P=0.0013$, ratio paired two-sided t -test. NS, not significant ($P=0.9865$).

Figure 5. Recognition of H4K20me0 is a prime function of BARD1 in HR. **a**, Western blot analysis of *BARD1*^{AID/AID} HCT116 cells at indicated time points following the addition of doxycycline to stimulate OsTIR1 expression and auxin (IAA) to induce OsTIR1-dependent BARD1-AID proteolysis. Representative of 2 biological replicates, unprocessed blots in Supplementary Fig. 5. *Indicates non-specific bands. **b**, IAA-addition hypersensitizes *BARD1*^{AID/AID} HCT116 cells to Olaparib. Cells were seeded in the presence of doxycycline, IAA and Olaparib were added one day later and left for 7 days before staining with crystal violet. Representative of 2 biological replicates. **c, d**, Analysis of BARD1 ARD function in PARPi resistance as defined in *BARD1*^{AID/AID} HCT116 cells. After 24 hours in doxycycline, indicated cell lines were treated with IAA, or carrier (DMSO), before immunoblotting whole cell lysates or measuring growth in the presence of Olaparib as indicated. Western blot showing equal stabilization of endogenous BRCA1 by the expression of wild type and all mutant BARD1 transgenes, but not the control (GST) transgene (**c**). Representative of 2 biological replicates, unprocessed blots in Supplementary Fig. 5. *eBARD1 indicates a weak unspecific band and the size of exogenous BARD1. Olaparib sensitivity was determined by resazurin

cell viability assay 7 days following incubation with Olaparib (2-fold dilution range from 7.8 nM – 2 μ M) in the presence (left panels) or absence (right panels) of IAA (**d**). Mean with S.D., $n=3$ independent experiments. **e**, Model illustrating how BARD1 recognition of H4K20me0 licenses DSBs in sister chromatid for HR. BRCA1-BARD1 identifies post-replicative chromatin by recognition of H4K20me0 on new histones, hereby enabling the complex to oppose 53BP1 function when a sister chromatid can be used for homology-directed error-free repair of DSBs.

References

1. Moynahan, M.E. & Jasin, M. Mitotic homologous recombination maintains genomic stability and suppresses tumorigenesis. *Nat Rev Mol Cell Biol* **11**, 196-207 (2010).
2. Hustedt, N. & Durocher, D. The control of DNA repair by the cell cycle. *Nat Cell Biol* **19**, 1-9 (2016).
3. Prakash, R., Zhang, Y., Feng, W. & Jasin, M. Homologous recombination and human health: the roles of BRCA1, BRCA2, and associated proteins. *Cold Spring Harb Perspect Biol* **7**, a016600 (2015).
4. Bunting, S.F. *et al.* 53BP1 inhibits homologous recombination in Brca1-deficient cells by blocking resection of DNA breaks. *Cell* **141**, 243-254 (2010).
5. Zimmermann, M. & de Lange, T. 53BP1: pro choice in DNA repair. *Trends Cell Biol* **24**, 108-117 (2014).
6. Saredi, G. *et al.* H4K20me0 marks post-replicative chromatin and recruits the TONSL-MMS22L DNA repair complex. *Nature* **534**, 714-718 (2016).
7. Beck, D.B., Oda, H., Shen, S.S. & Reinberg, D. PR-Set7 and H4K20me1: at the crossroads of genome integrity, cell cycle, chromosome condensation, and transcription. *Genes Dev* **26**, 325-337 (2012).
8. Piwko, W., Buser, R. & Peter, M. Rescuing stalled replication forks: MMS22L-TONSL, a novel complex for DNA replication fork repair in human cells. *Cell Cycle* **10**, 1703-1705 (2011).
9. Piwko, W. *et al.* The MMS22L-TONSL heterodimer directly promotes RAD51-dependent recombination upon replication stress. *EMBO J* **35**, 2584-2601 (2016).
10. Botuyan, M.V. *et al.* Structural basis for the methylation state-specific recognition of histone H4-K20 by 53BP1 and Crb2 in DNA repair. *Cell* **127**, 1361-1373 (2006).

11. Chapman, J.R., Sossick, A.J., Boulton, S.J. & Jackson, S.P. BRCA1-associated exclusion of 53BP1 from DNA damage sites underlies temporal control of DNA repair. *J Cell Sci* **125**, 3529-3534 (2012).
12. Pellegrino, S., Michelena, J., Teloni, F., Imhof, R. & Altmeyer, M. Replication-Coupled Dilution of H4K20me2 Guides 53BP1 to Pre-replicative Chromatin. *Cell Rep* **19**, 1819-1831 (2017).
13. Simonetta, M. *et al.* H4K20me2 distinguishes pre-replicative from post-replicative chromatin to appropriately direct DNA repair pathway choice by 53BP1-RIF1-MAD2L2. *Cell Cycle* **17**, 124-136 (2018).
14. Uckelmann, M. & Sixma, T.K. Histone ubiquitination in the DNA damage response. *DNA Repair* **56**, 92-101 (2017).
15. Raschle, M. *et al.* DNA repair. Proteomics reveals dynamic assembly of repair complexes during bypass of DNA cross-links. *Science* **348**, 1253671 (2015).
16. Kuo, A.J. *et al.* The BAH domain of ORC1 links H4K20me2 to DNA replication licensing and Meier-Gorlin syndrome. *Nature* **484**, 115-119 (2012).
17. Fox, D., 3rd *et al.* Crystal structure of the BARD1 ankyrin repeat domain and its functional consequences. *J Biol Chem* **283**, 21179-21186 (2008).
18. Tuzon, C.T. *et al.* Concerted activities of distinct H4K20 methyltransferases at DNA double-strand breaks regulate 53BP1 nucleation and NHEJ-directed repair. *Cell Rep* **8**, 430-438 (2014).
19. Karanam, K., Kafri, R., Loewer, A. & Lahav, G. Quantitative live cell imaging reveals a gradual shift between DNA repair mechanisms and a maximal use of HR in mid S phase. *Mol Cell* **47**, 320-329 (2012).
20. Wilson, M.D. *et al.* The structural basis of modified nucleosome recognition by 53BP1. *Nature* **536**, 100-103 (2016).
21. Pierce, A.J., Johnson, R.D., Thompson, L.H. & Jasin, M. XRCC3 promotes homology-directed repair of DNA damage in mammalian cells. *Genes Dev* **13**, 2633-2638 (1999).
22. Laufer, M. *et al.* Structural requirements for the BARD1 tumor suppressor in chromosomal stability and homology-directed DNA repair. *J Biol Chem* **282**, 34325-34333 (2007).
23. Jackson, S.P. & Helleday, T. Drugging DNA repair. *Science* **352**, 1178-1179 (2016).
24. Densham, R.M. *et al.* Human BRCA1-BARD1 ubiquitin ligase activity counteracts

- chromatin barriers to DNA resection. *Nat Struct Mol Biol* **23**, 647-655 (2016).
25. Natsume, T., Kiyomitsu, T., Saga, Y. & Kanemaki, M.T. Rapid Protein Depletion in Human Cells by Auxin-Inducible Degron Tagging with Short Homology Donors. *Cell Rep* **15**, 210-218 (2016).
 26. Li, M. & Yu, X. Function of BRCA1 in the DNA damage response is mediated by ADP-ribosylation. *Cancer Cell* **23**, 693-704 (2013).
 27. Billing, D. *et al.* The BRCT Domains of the BRCA1 and BARD1 Tumor Suppressors Differentially Regulate Homology-Directed Repair and Stalled Fork Protection. *Mol Cell* (2018).
 28. Shakya, R. *et al.* BRCA1 tumor suppression depends on BRCT phosphoprotein binding, but not its E3 ligase activity. *Science* **334**, 525-528 (2011).
 29. Huertas, P., Cortes-Ledesma, F., Sartori, A.A., Aguilera, A. & Jackson, S.P. CDK targets Sae2 to control DNA-end resection and homologous recombination. *Nature* **455**, 689-692 (2008).
 30. Orthwein, A. *et al.* A mechanism for the suppression of homologous recombination in G1 cells. *Nature* **528**, 422-426 (2015).
 31. Huang, T.H. *et al.* The Histone Chaperones ASF1 and CAF-1 Promote MMS22L-TONSL-Mediated Rad51 Loading onto ssDNA during Homologous Recombination in Human Cells. *Mol Cell* (2018).
 32. Ochs, F. *et al.* 53BP1 fosters fidelity of homology-directed DNA repair. *Nat Struct Mol Biol* **23**, 714-721 (2016).
 33. Wang, B. *et al.* Abraxas and RAP80 form a BRCA1 protein complex required for the DNA damage response. *Science* **316**, 1194-1198 (2007).
 34. Doil, C. *et al.* RNF168 binds and amplifies ubiquitin conjugates on damaged chromosomes to allow accumulation of repair proteins. *Cell* **136**, 435-446 (2009).
 35. Stewart, G.S. *et al.* The RIDDLE syndrome protein mediates a ubiquitin-dependent signaling cascade at sites of DNA damage. *Cell* **136**, 420-434 (2009).
 36. Escribano-Diaz, C. *et al.* A cell cycle-dependent regulatory circuit composed of 53BP1-RIF1 and BRCA1-CtIP controls DNA repair pathway choice. *Mol Cell* **49**, 872-883 (2013).
 37. Westermarck, U.K. *et al.* BARD1 participates with BRCA1 in homology-directed repair of chromosome breaks. *Mol Cell Biol* **23**, 7926-7936 (2003).

38. Zaware, N. & Zhou, M.M. Chemical modulators for epigenome reader domains as emerging epigenetic therapies for cancer and inflammation. *Curr Opin Chem Biol* **39**, 116-125 (2017).

Materials and Methods

Preparation of recombinant histones

Recombinant human core histone proteins were expressed in *E. coli* BL21(DE3)/RIL cells from pET21b(+) (Novagen) vectors and purified by denaturing gel filtration and ion exchange chromatography essentially as described³⁹.

Preparation of truncated histone H4 for native chemical ligations

Truncated human H4 Δ 1-28I29C protein for ligations of modified histone H4 was expressed from a pET24b(+) vector (Novagen) in *E. coli* BL21(DE3)/RIL cells. The insoluble protein was extracted from inclusion bodies with Unfolding buffer (20 mM Tris [pH 7.5], 7 M Guanidine HCl, and 100 mM DTT) for 1 hr at room temperature and the cleared supernatant loaded on a Sephacryl S200 gel filtration column (GE Healthcare) in SAU-1000 (20 mM NaAcetate [pH 5.2], 7 M Urea, 1 M NaCl, and 1 mM EDTA) without any reducing agents. H4 Δ 1-28I29C containing fractions were combined and further purified on a reversed phase chromatography column (Perkin Elmer Aquapore RP-300 C8 250x4.6 mm i.d.) using a gradient of 0-65% B (Buffer A: 0.1% trifluoroacetic in water; B: 90% acetonitrile, 0.1% trifluoroacetic) over 20 column volumes. Fractions containing pure H4 Δ 1-28I29C were pooled and lyophilized.

Native chemical ligation

Native chemical ligations were carried out in 550 μ l of degassed ligation buffer (200 mM KPO₄, 2 mM EDTA, 6 M Guanidine HCl) containing 1 mg of modified/unmodified H4 peptides spanning aa's 1-28 and containing a C-terminal thioester (Cambridge Peptides), 4 mg of truncated H4 Δ 1-28I29C, 20 mg 4-Mercaptophenylacetic acid (MPAA) and 25 mg TCEP as reducing agent at a pH of 7.5. The reactions were incubated over night at 40°C and quenched by addition of 60 μ l 1 M DTT and 700 μ l 0.5% acetic acid. After precipitation clearance by centrifugation, the ligation reactions were directly loaded and purified on a reversed phase chromatography column (Perkin Elmer Aquapore RP-300 C8 250x4.6 mm i.d.) using a gradient of 35-45% B (Buffer A: 0.1% trifluoroacetic in water; B: 90% acetonitrile, 0.1% trifluoroacetic) over 10 column volumes. Positive fractions containing ligated full-length histone H4 were combined and directly lyophilized.

Nucleosome assembly

Histone octamers were refolded from the purified histones and assembled into nucleosomes with

biotinylated DNA via salt deposition dialysis as previously described³⁹. Biotinylated nucleosomal DNAs containing two 601 nucleosome positioning sequences separated by a 50 bp linker (di-nucleosomes) were prepared as described³⁹. Di-nucleosomes were assembled in the presence of MMTV A competitor DNA and a slight excess of octamers to ensure saturation of the 601 repeats. The reconstituted di-nucleosomes were then immobilized on Streptavidin Sepharose HP beads (GE Healthcare) via the biotinylated DNA, washed to remove MMTV A competitor DNA and MMTV A nucleosomes, and directly used for SILAC nucleosome affinity purifications. Correct assembly and immobilization of nucleosomes were verified by native PAGE.

SILAC nucleosome affinity purifications (SNAP)

SILAC-labelled nuclear extracts were prepared from HeLa S3 cells as previously described³⁹. For each pull-down, nucleosomes corresponding to 12.5 µg of octamer were immobilized on 10 µl Streptavidin Sepharose HP beads (GE Healthcare) in the final reconstitution buffer (10 mM Tris [pH 7.5], 250 mM KCl, 1 mM EDTA and 1 mM DTT; supplemented with 0.1% NP40) and then rotated with 0.5 mg HeLa S3 SILAC-labelled nuclear extract in 1 ml of SNAP buffer (20 mM HEPES [pH 7.9], 150 mM NaCl, 0.2 mM EDTA, 10% Glycerol) supplemented with 0.1% NP40, 1 mM DTT and protease inhibitors cocktail (Roche) for 4 hr at 4°C. After two washes with 1 ml SNAP buffer +0.1% NP40 followed by two washes with 1 ml SNAP buffer without NP40, the beads from both SILAC pull-downs were pooled. The supernatant was completely removed, and bound proteins were eluted by on-bead digestion.

On-bead digestion and peptide purification

The beads were resuspended in 50 µl of Elution buffer (2M Urea, 100 mM Tris [pH 7.5], 10 mM DTT) and incubated on a shaker (1,000 rpm) at 25°C for 20 min. Iodoacetamide (Sigma I1149) was added to a final concentration of 50 mM and the sample was incubated on a shaker (1,000 rpm) at 25°C in the dark for 10 min. After digestion with 0.3 µg Trypsin (Promega V5113) for 2 hr on a shaker (1,000 rpm) at 25°C, the supernatant was transferred to a new tube and was further digested with 0.1 µg Trypsin overnight at 25°C. The digestion was stopped by adding 5.5 µl of 10% TFA. Eluted peptides were purified on C18 stage-tips (Glygen 10-200 µL TopTips) following the manufacturer's instructions and dried with a SpeedVac.

Mass Spectrometry

Samples were loaded at 8 µl/min onto a trap column (Thermo Scientific Acclaim Pepmap 100; 100

µm internal diameter, 2 cm length, C18 reversed-phase material, 5 µm diameter beads, 100 Å pore size) in 2% acetonitrile, 0.1% trifluoroacetic acid.

Peptides were eluted on-line to an analytical column (Thermo Scientific Acclaim Pepmap RSLC; 75 µm internal diameter, 25 cm length, C18 reversed-phase material, 2 µm diameter beads, 100 Å pore size) and separated using a flow rate of 250 nl/min and gradient conditions of: Initial 5 minutes with 4% buffer B, then 90 minutes gradient 4-25% B, then 30 minutes gradient 25-45% B, then 1 minute gradient 45-90% B and finally 15 minutes isocratic at 100% B before returning to starting conditions for a 15 minute equilibration (Buffer A: 2% acetonitrile, 0.1% formic acid in water; B: 80% acetonitrile, 0.1% formic acid).

The QExactive instrument acquired full scan survey spectra (m/z 300 to 1650) at 70,000 resolution. An AGC target value of 3E6 and a maximum injection time of 20 milliseconds were used. The top 10 most abundant multiply-charged ions were selected in a data-dependent manner, fragmented by higher-energy collision-induced dissociation (HCD) and data were collected over the range 200-2000 m/z at 17,500 resolution. An AGC target value of 1E5 with a maximum injection time of 120 milliseconds were used. A dynamic exclusion time of 30 seconds was enabled.

Mass Spectrometry Data Processing

Protein abundances from the QExactive mass spectrometer were quantified by MaxQuant 1.6.0.16 using 2-plex labeling (Arg10 and Lys8). The search was run against human UP000005640 proteome (version GCA_000001405.26) from UniProt. Search parameters were set up to allow variable oxidation on methionines and acetylation on N-termini as well as fixed carbamidomethylation on cysteines. Tryptic peptides with up to 2 missed cleavages were considered for analysis and tolerance settings were set to Orbitrap instrument. Co-fragmented peptide identification and matching between runs has been enabled. For protein quantification, minimum ratio count was set to 1 and remaining settings left default. The normalised H/L ratios in proteinGroups.txt file output by MaxQuant have been transformed to log2 scale for further processing. Each protein in the dataset containing Ankyrin repeat-containing domain has been identified using information from InterPro superfamily IPR036770. Twenty-six proteins that were marked as either "Potential contaminant", "Reverse" or "Only identified by site" by MaxQuant were dropped from the dataset (i.e. 1.81% of data). Further 76 proteins (5.39% of the remaining data), were dropped because they had only forward, or reverse ratio, but not complete pairs. The data presented in Figure 1a are zoomed in to log2 fold-change

ratios below the value of 5, thus excluding four outlier proteins (SPTA1, STAG2, histone H3 and histone H4) that are not enriched in either nucleosome pull-down. The full proteomics list for H4K20me0/me2 nucleosome pull-downs is presented in Supplementary Table 1.

Di-nucleosome pull-down assay. Biotinylated di-nucleosomes carrying H4K20me0 or H4K20me2, or biotin only as control, were mixed with MyOne T1 streptavidin beads (ThermoFisher) in Coupling Buffer (10 mM Tris-HCl, 1 mM EDTA, 250 mM KCl). Di-nucleosomes and beads were incubated for 1 hr at 4°C on a rotating shaker to allow the coupling and, subsequently, washed twice with SNAP buffer (20 mM HEPES, 150 mM NaCl, 0.2 mM EDTA, 10% glycerol, 0.1% NP-40). At the same time, 320-450µg of HeLa cell nuclear extracts were incubated with 10 µg ml⁻¹ Herring Sperm DNA (Sigma) in SNAP buffer (final volume, 900 µl) and allowed to rotate for 1 hr at 4°C. Inputs of 2% of the extracts were taken before diluting each sample with SNAP buffer. The extracts were then added to the washed di-nucleosome-coupled beads and incubated 4 hr, rotating at 4°C. The beads were then washed with 4× 900 µl Wash Buffer (20 mM HEPES, 500 mM NaCl, 0.2 mM EDTA, 10% glycerol, 0.25% NP-40, supplemented with 10 µg ml⁻¹ Herring Sperm DNA) for 2 min at 4°C. After the last wash, the beads were carefully dried and boiled in 20 µl 1X LSB. Pull-downs were visualized by western blotting after protein separation on a NuPAGE 4-12% Bis-Tris gradient gel (ThermoFisher).

Cell culture, transfection and drug treatment

U-2-OS (gift from J. Bartek), HeLa S3 (gift from P. Nakatani) and HCT116 (gift from Dr. Ian Tomlinson) cells were grown in DMEM (Gibco) containing 10% FBS (Hyclone) and 1% penicillin/streptomycin and drugs for selection. Cells inducible for Flag-HA-BARD1 WT and ARD mutants were generated in Flp-In T-Rex U-2-OS cells (Invitrogen) by transfection of pcDNA5/FRT/TO-Flag-HA-BARD1 plasmids with Lipofectamine 2000, according to the manufacturer's protocol, and selection with hygromycin (200 µg/ml). Flag-HA-BARD1 cDNA contains silent point mutations that render it resistant to siRNA siBARD1 (see below). All cell lines were authenticated by western blotting and/or immunofluorescence. All cell lines used in this study tested negative for mycoplasma contamination. Expression of Flag-HA-BARD1 was induced by addition of 1 µg/ml of tetracycline for 24-48 hours. For transient expression of Flag-HA-BARD1,

expression plasmids were introduced by transfection with Lipofectamine 2000 (Invitrogen) according to the manufacturer's protocol and cells harvested 24-48 hours post-transfection. To establish a parental cell line expressing the E3 ubiquitin ligase OsTIR1, HCT116 male colorectal carcinoma cells were simultaneously transfected with a version pX330 (Addgene plasmid: #42230) containing a locus-specific gRNA targeting AAVS1 (5'-GGGGCCACTAGGGACAGGAT-3') and pMK243 Tet-OsTIR1 (Addgene plasmid: #72835) using Fugene HD (Promega). Individual sub-clones were isolated and assessed for doxycycline inducible expression by western blot using an OsTIR1-specific antibody (a gift from M. Kanemaki, NIG). Integration of Tet-OsTIR1 at the AAVS1 locus was confirmed by PCR. siRNA transfection was performed with RNAiMax reagent (Invitrogen) according to the manufacturer's protocol. siRNA sequences (Sigma): siBARD1: 5' - AAGCUGUUGCCCAUAUGGCU -3' , siRNF8: 5'- UGCGGAGUAUGAAUAUGAA -3', si53BP1: 5'- GAAGGACGGAGUACUAAUA -3' The SET8 siRNAs have been previously described⁶.

AID tagging of endogenous BARD1 in Tet-OsTIR1 HCT116 cells

One day prior to transfection, 3.2×10^5 Tet-OsTIR1 HCT116 cells were seeded in a single well of a 6-well plate. 800 ng of pX330 containing a gRNA specific to the C-terminus of BARD1 (5'-TATAATATTCAGCTGTCAAG-3') was combined with 600 ng of circular donor plasmid and transfected using Fugene HD (Promega) according to the manufacturer's protocol. After 48 h selection in blasticidin (10 µg/ml), surviving cells were seeded at low density in a 10 cm dish for sub-cloning. Genomic DNA was isolated from individual clones following expansion and bi-allelic integration of the AID tag and selection cassette was assessed by PCR with primers flanking the integration site (BARD1_IntegrationScreen_R: 5'-GCATTCATTTTATGTTTCAGGTTTCAGG-3' and BARD1_IntegrationScreen_F: 5'-CTGTTTGATGGATGCTACTTCTATTTG-3'). Individual alleles of promising clones were TA cloned into pJET 1.2 and sequenced to ensure clonal purity. Complementation of confirmed *BARD1*^{AID/AID} clones was carried out by stable transduction using lentivirus.

Donor plasmid construction:

A donor plasmid for endogenous AID tagging of the BARD1 C-terminus were constructed by

overlapping fusion PCR of 3 fragments: 1) a left homology arm of 233 bp amplified from HCT116 genomic DNA using oligos BARD1_LHomArm_F (5'-GTGACTCAGACCATCAATACAG-3') and BARD1_LHomArm_R (5'-TCTTTAGGACAAGCACTCTTCTCCTTGGCGCCTGCACCGCTGTCAAGAGGAAGCAACTCAAATGAC-3'), 2) a right homology arm of 257 bp amplified from HCT116 genomic DNA using oligos BARD1_RHomArm_R (5'-GCAATCCCAGCTTCTAAATGGTAAAC-3') and BARD1_RHomArm_F (5'-ATTAGGTCCCTCGAAGAGGTTCACTAGGATCCGGTACCCAAGTTGCTTCCTCTTGACAGCTG-3'), and 3) an AID tag and blasticidin selection cassette amplified from pMK288 (Addgene plasmid #72826)(REF: PMID 27052166) using oligos BARD1_AIDCassette_F (5'-CGGTGCAGGCGCCAAGGAGAAGAGTG-3') and BARD1_AIDCassette_R (5'-TGGGTACCGGATCCTAG-3'). All three fragments were fused in a PCR reaction containing BARD1_LHomArm_F and BARD1_RHomArm_R and the fused product was ligated into pJET 1.2 by blunt end cloning following the CloneJET PCR Cloning Kit manufacturer's protocol (Thermo Fisher Scientific).

Immunofluorescence, microscopy and ionizing irradiation

U-2-OS cells conditional for Flag-HA-BARD1 were grown on glass coverslips or 96 well plate and either directly fixed in 4% paraformaldehyde (PFA) for 10 mins or washed in CSK, pre-extracted 5 min with CSK/0.5% Triton X-100 (on ice) and rinsed with CSK and PBS before fixation in 4% PFA for 10 mins. For high content quantitative analysis, fluorescence images were acquired using an Olympus ScanR high-content microscope and processed on the ScanR analysis software. More than 5000 cells per sample were analysed. Cell cycle phases were gated on DAPI and EdU intensity. For co-localization analysis by deconvolution microscopy, images were acquired on a DeltaVision microscope with a 60x oil objective and analysed by SoftWoRX 6.5.2. Pearson coefficient correlation analysis was performed on single cells using SoftWoRX 6.5.2. Ionizing radiation treatment was given using an x-ray apparatus (Faxitron) calibrated to give 1 Gy per 1 min. For analysis of DNA end resection, BrdU labeling and detection under non-denaturing conditions was performed as previously described¹². Briefly, U-2-OS cells were pre-incubated with 30 μ M BrdU for 24 h and then treated with IR (3 Gy). After 3 h recovery, cells were pre-extracted with nuclear

extraction buffer (20 mM HEPES-NaOH [pH 7.5], 20 mM NaCl, 5 mM MgCl₂, 1 mM DTT, 0.5% NP-40, 100 μM PMSF, 10 μM Pepstatin, 10 μM Leupeptin, 0.2 mM Na₃VO₄, 10 mM β-Glycerophosphate, 5 mM NaF) on ice for 10 min and fixed with 4% formaldehyde/PBS on ice for 10 min.

HR assay

DR-GFP-U-2-OS or BARD1-null mouse mammary carcinoma cells (18-09) were used as described previously^{21, 22}. Briefly, 2.5-5×10⁵ cells/well were seeded on 6-well plates. After 24 h, the cells were transfected with 1 μg of I-SceI expression vector (pCBASce), 2 μg of BARD1 expression vector or empty vector, 1 μg of RFP expression vector. 24 h after transfection, the cells were washed and replated on 100-mm dishes. Flow cytometric analysis to quantify the presence of GFP-positive cells was performed 2 days later on a FACSCalibur using Cellquest Pro software (BD Biosciences). For each sample, 30,000 cells were assessed, and the percentage of GFP-positive cells in RFP positive cells was calculated as HR repaired cells. RFP-encoding vector was used to provide a control for transfection efficiency. For 53BP1 depletion, the siRNAs were transfected 24 h prior to plasmid transfection.

Clonogenic assay

U-2-OS inducible for FLAG-HA-BARD1 WT and ARD 3A mutant were seeded in technical triplicates of 300 to 10,000 cells in the presence or absence of tetracycline. After 48 h, Olaparib (Selleckchem, S1060) was added for 72 h. Cells were then cultured in fresh medium for 7–15 days before fixation and staining with MeOH/Crystal Violet. For the complementation, BARD1 WT and ARD 3A mutant cells were transfected with siRNA and seeded with or without tetracycline. The cells were trypsinised 24 h later and seeded in technical triplicates of 300 to 10,000 cells in the presence or absence of tetracycline. After 24 h, Olaparib was added for 24 hours as indicated concentration. Cells were then cultured in fresh medium for 7–15 days before fixation and staining with MeOH/Crystal Violet. Colony formation efficiency was determined by manual colony counting and normalized to non-drug treated control. Each data point represents a technical triplicate of seeded cells within each biological replicate.

Resazurin cell viability assay

300 Tet-OsTIR1 HCT116 cells per well were seeded in triplicate in 96 well plates in the presence of doxycycline (1 mg/ml) for each concentration of Olaparib (Selleckchem, S1060). 24 h after plating, IAA was added to a final concentration of 1 mM. 1 h after the addition of IAA, Olaparib was added to the indicated final concentrations. Medium was refreshed at 4 days. 7 days after the addition of Olaparib, medium was replaced with phenol red-free DMEM (10% FBS, 1% penicillin/streptomycin) containing 10 mg/ml Resazurin and the plates were incubated for 2 h. The relative fluorescence intensity of each well was then measured using a BMG LABTECH CLARIOstar plate reader equipped with a 560 nm excitation / 590 nm emission filter set.

Antibodies

The following antibodies were used for western blot: BARD1 (Bethyl A300-263A, 1:500), BARD1 (Abcam ab64164, 1:500), SLF1 (Novus Biologicals NBP1-88358, 1:500), HA (HA.11, BioLegend 901513, previously Covance MMS-101P, 1:500), H4K20me2 (Diagenode C15200205, 1:3000), GFP (Roche 11 814 460 001, mixture of clones 7.1 and 13.1, 1:500), SET8 (Millipore, 06-1304, 1:1000), OsTIR1 (a gift from Masato Masato T. Kanemaki, 1:1000), Actin (Sigma A1978, 1:2000) and BRCA1 (Santa Cruz Biotechnology sc-6954, clone 9, 1:400). The following antibodies were used for immunofluorescence: BARD1 (Bethyl A300-263A, 1:500), BRCA1 (Santa Cruz Biotechnology sc-6954, clone 9, 1:400), 53BP1 (Santa Cruz Biotechnology H-300, 1:500), H4K20me1 (Abcam ab9051, 1:250; validated in Supplementary Fig. 2g), H4K20me2 (Diagenode C15200205, 1:250; validated in Supplementary Fig. 2g), H4K20me0 (Abcam ab227804, 1:10000; validated in Supplementary Fig. 2g), Phospho-H2A.X (S139) (Cell Signalling Technology 2577, 1:1000), HA (Roche 1 867 423, 1:200), HA (Bio Legend 901509, 1:100), BrdU (Eurobio ABC117-7513, 1:1000), and MCM2 (BD Biosciences 610701, 1:150).

Modelling the structure of BARD1 bound to histone H4

The Rosetta macromolecular modelling package (www.rosettacommons.org), which have proven successful in a variety of protein design applications involving protein structure predictions,

predictions of protein-protein and protein-peptide interfaces was used to model the interaction of the histone H4 tail with BARD1. Due to the high structural similarity of TONSL (PDBID: 5JA4) and BARD1 ARD (PDBID: 3C5R) (main chain RMSD = 0.96 Å), we chose to use the structure of TONSL in complex with the histone H3-H4 tetramer as a seed structure to model the complex the histone H4 tail bound to BARD1. The starting structure for the Rosetta refinement of BARD1 bound to histone H4 was prepared from the structural superposition of the ARD domains of TONSL and BARD1. Analysis of the TONSL ARD and histone H4 interaction interface (PDBID: 5JA4) suggest that the imidazole side chain of H18 (in H4) is positively charged, as it is located in a cavity between the negatively charged residues E568 and D604 which is conserved (E467 and D500) in the ARD domain of BARD1. A positively charged H18 was also supported by pKa calculations using the Rosetta protocol to calculate pKa values. As histidines in Rosetta by default are assumed to be neutrally charged, we prepared a parameter file to protonate both the epsilon and delta state of H18 to carry a net (+1) positive charge. The preliminary model of the BARD1 and H3-H4 complex was exhaustively refined using Rosetta 5.0.37 by subjecting it to 3,000 steps of full-atom structure relaxation (in the Rosetta force-field) which samples side chain and backbone conformational changes, similar to those suggested to underlie observed conformational heterogeneity in high-resolution crystal structures to broadly sample the protein-protein interface and the conformational variability of the complex⁴⁰. For each relax cycle, five rounds of repacking followed by gradient base minimization in torsion space (backbone ϕ/ψ and side chain χ torsional degrees of freedom) was performed until convergence (absolute score change upon minimization of less than one REU Rosetta Energy Unit). From om all cycles performed the best scoring pose was selected to represent the structure of BARD1 bound to the histone H4 tail shown in Supplementary Fig. 4a.

Statistics and Reproducibility

Statistics were analysed with GraphPad Prism 7. All statistics were evaluated by either independent or paired two-tailed Student's *t*-test and two-tailed Mann-Whitney test. Pearson's correlation and Student's *t*-test were performed under the assumption of normality. The exact sample sizes (n) used to calculate statistics are provided in the figure legends. *P* values are provided and defined in the legend of the figures. Whiskers indicate 10-90 percentile and outliers are plotted as individual points in box-and-whisker plot. All experiments were reproduced with similar results as a minimum two times.

Code availability

The code used for analysis of mass spectrometry data is publicly available at GitHub (<https://github.com/lukauskas/publications-nakamura-2018-snap-h4k20me2>).

Data availability

The mass spectrometry proteomics data have been deposited to the ProteomeXchange Consortium via the PRIDE partner repository with the dataset identifier PXD009281 and is presented in Supplementary Table 1. Unprocessed images of all gels and blots (Fig. 1c, d, Fig. 5a, c; Supplementary Fig. 2h) are provided in Supplementary Fig. 5. Source data for all graphs are provided in Supplementary Table 2. All other data supporting the findings of this study are available from the corresponding authors on reasonable request.

References for Methods

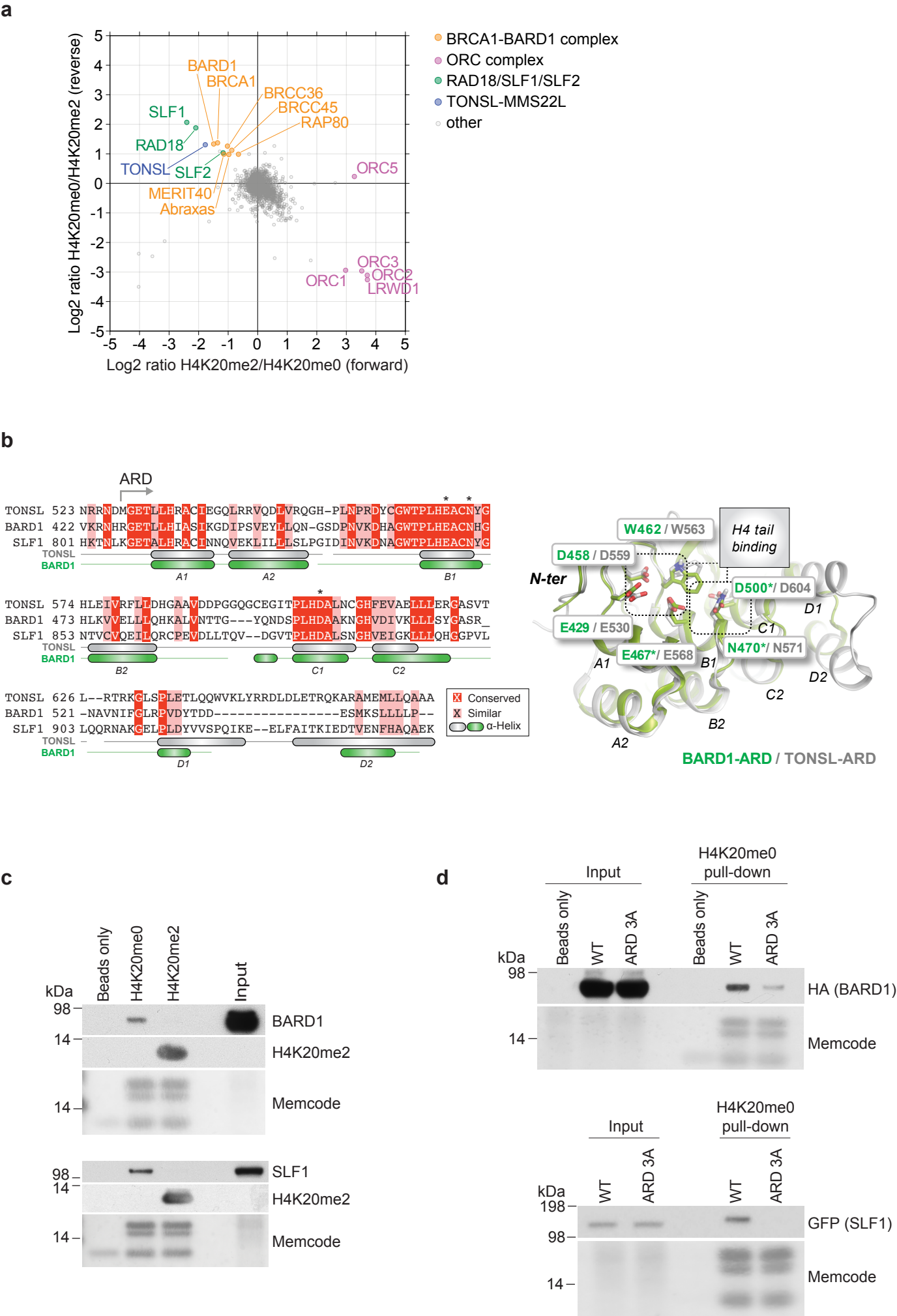
39. Bartke, T. *et al.* Nucleosome-interacting proteins regulated by DNA and histone methylation. *Cell* **143**, 470-484 (2010).
40. Conway, P., Tyka, M.D., DiMaio, F., Konerding, D.E. & Baker, D. Relaxation of backbone bond geometry improves protein energy landscape modeling. *Protein Sci* **23**, 47-55 (2014).

Type of file: figure

Label: 1

Filename: figure_1.pdf

Figure 1

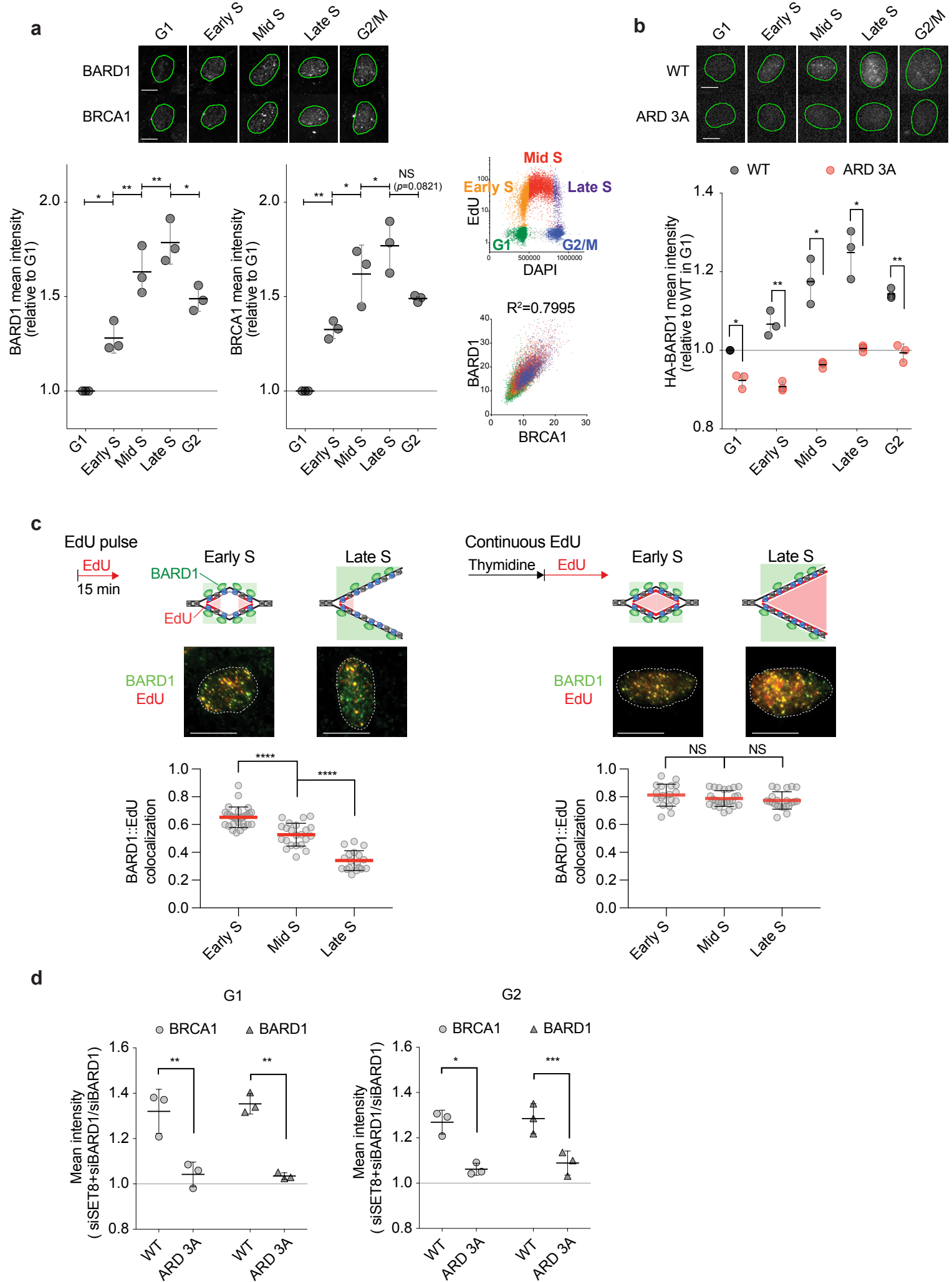


Type of file: figure

Label: 2

Filename: figure_2.pdf

Figure 2

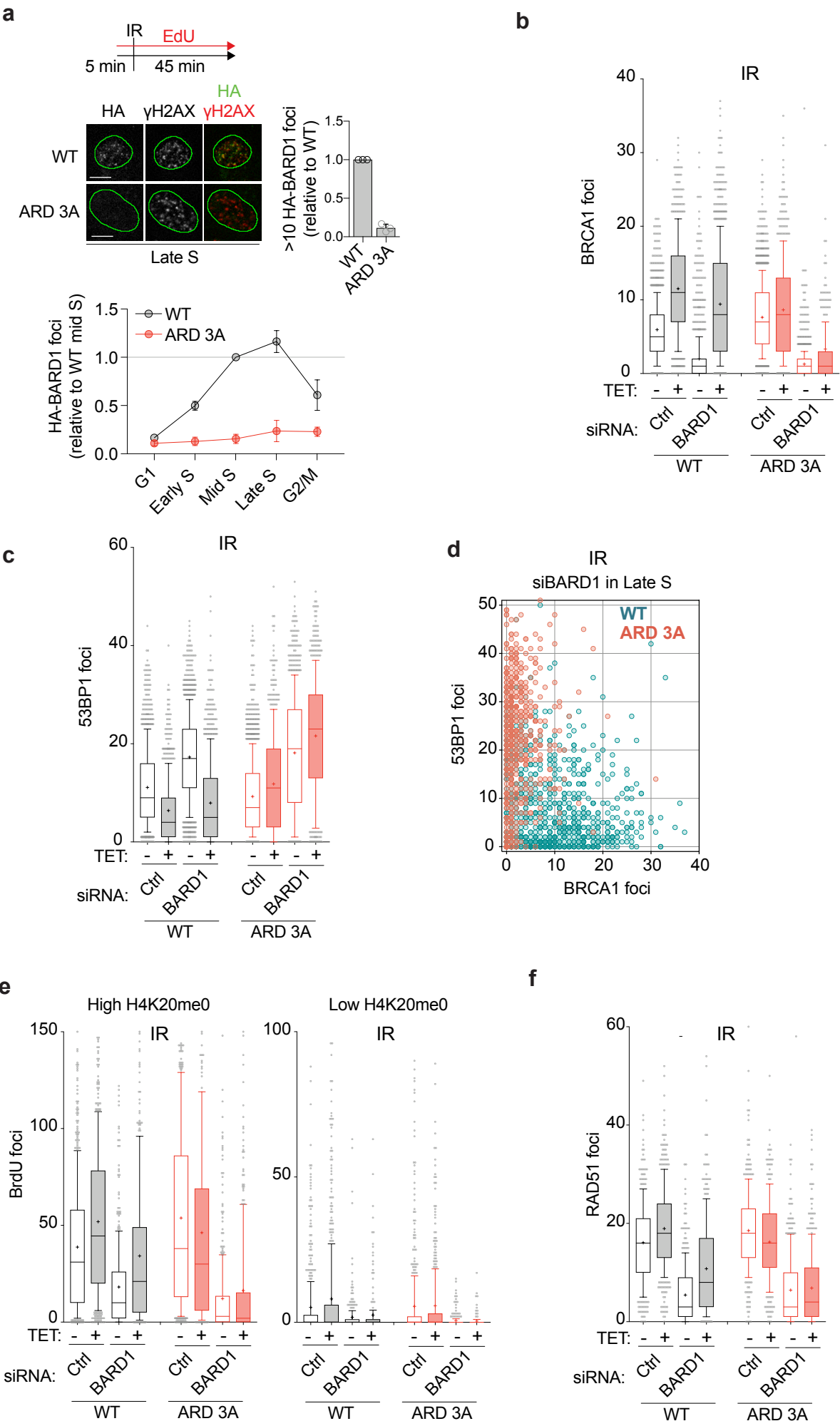


Type of file: figure

Label: 3

Filename: figure_3.pdf

Figure 3

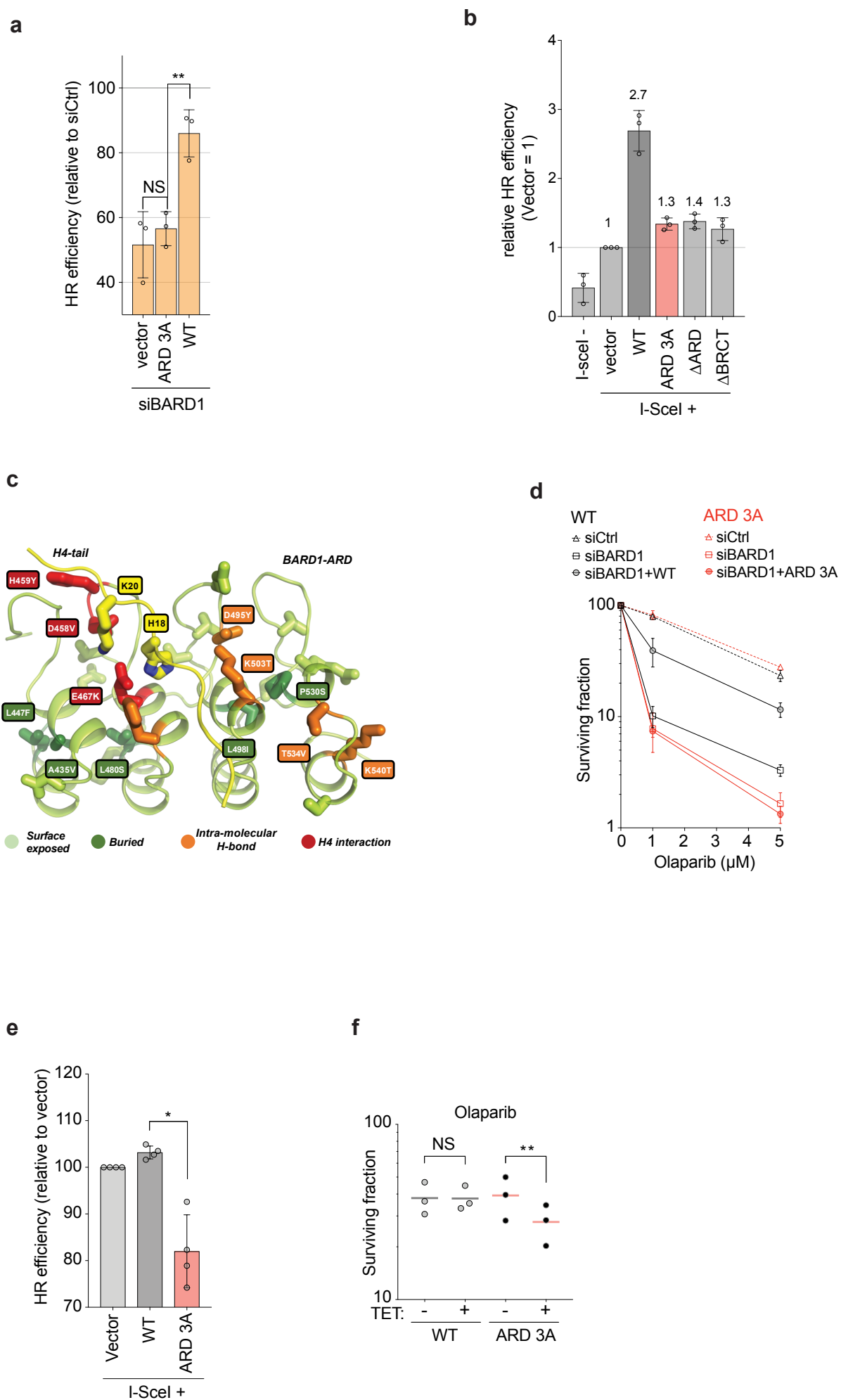


Type of file: figure

Label: 4

Filename: figure_4.pdf

Figure 4

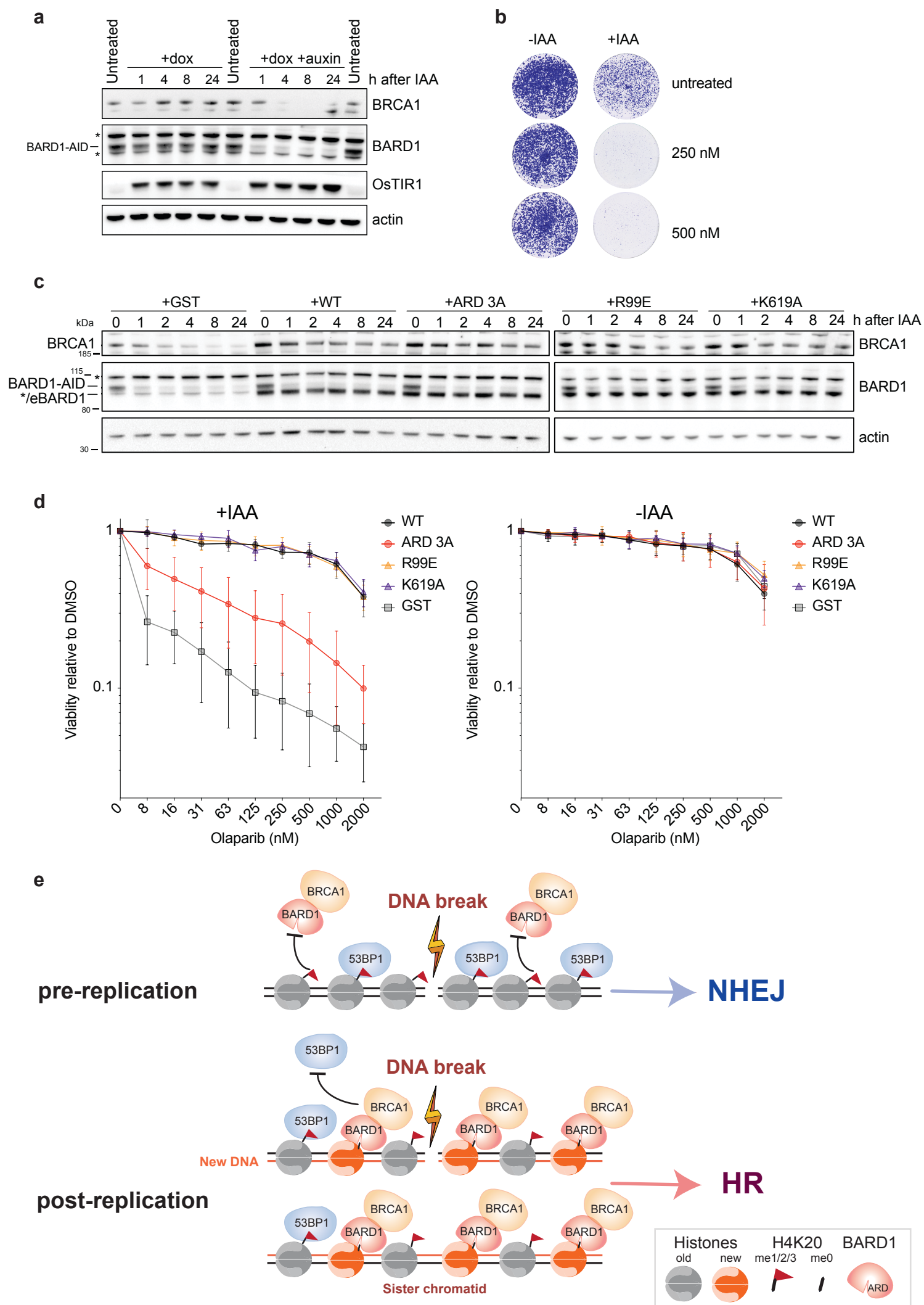


Type of file: figure

Label: 5

Filename: figure_5.pdf

Figure 5



Europe PMC plus has received the file 'supp_info_1.docx' as supplementary data. The file will not appear in this PDF Receipt, but it will be linked to the web version of your manuscript.

Europe PMC plus has received the file 'supp_info_2.pdf' as supplementary data. The file will not appear in this PDF Receipt, but it will be linked to the web version of your manuscript.